Quantum Molecular Dynamics Simulations of Low-Temperature High Energy Density Matter: Solid p-H_2/Li and p-H_2/B

Soonmin Jang, Seogjoo Jang, and Gregory A. Voth*

Department of Chemistry and Henry Eyring Center for Theoretical Chemistry, University of Utah, 315 S. 1400 E. Rm Dock, Salt Lake City, Utah 84112-0850

Received: June 23, 1999; In Final Form: September 8, 1999

The metastability of atomic impurities, Li and B, trapped in solid parahydrogen is studied by employing path integral molecular dynamics (PIMD) and centroid molecular dynamics (CMD) simulations at 4 K and zero external pressure. Starting from pure solid hydrogen consisting of 1440 particles, doped systems are prepared by substituting impurity atoms for hydrogen molecules at substitutional defect sites. For various concentrations, thermodynamic quantities are then calculated and the stability of the systems is monitored. For the case of lithium, systems containing 2.5 mol % dopants remain metastable with convergent thermodynamic quantities, but systems with 3.3 mol % or more dopants become unstable. For the case of boron, systems containing as high as 15 mol % dopants remain metastable on the time scale of the simulation, while systems with 25 mol % dopants do not. These results provide evidence of the transition from metastability to global instability and a rough estimate of the maximum doping density of the two atomic species. The calculations show that boron-doped systems have the potential to achieve a higher impurity concentration than lithium-doped systems. The intrinsic boron reaction rate at longer times was calculated for 6.25 mol % of boron impurities. The quantum centroid potential of mean force (PMF) was calculated and then the recombination reaction rate was estimated using path integral quantum transition state theory (PI-QTST). The PI-QTST calculation suggests that the transition state for boron dimer recombination at this concentration occurs at 5.39 Å separation and its free energy barrier is 360 ± 36 K. The calculated intrinsic recombination reaction rate is approximately 8×10^{-27} s^{-1}. This result suggests that the overall reaction rate of boron recombination reaction may be limited by the intrinsic recombination rate rather than by self-diffusion of the impurities. It is also found that the initial reaction of boron induces only local recombination of other boron impurities at this concentration and not a global instability. The dynamical effect of a single boron pair reaction on the rest of the system has also been studied by CMD simulations. These simulations show that the energy release from the dimer recombination does not lead to global melting of the solid.

I. Introduction

Solid parahydrogen is one of the simplest quantum solids and has been the subject of many theoretical and experimental studies. Experimental evidence shows that impurity atoms such as Li, B, and F can be metastably trapped in the solid hydrogen matrix, suggesting its potential usage as high energy density matter (HEDM).[1−3] Classical molecular dynamics (MD) simulation is not suitable for these systems because of the substantial quantum behavior of the host and guest molecules. To date, various quantum simulations have been performed, but they have been mostly confined to pure solid parahydrogen or hydrogen systems containing at most two lithium impurities.[4−8] For boron atoms with parahydrogen, there have been simulation studies on the stability of small $B(H_2)_n$ clusters,[9,10] and it is suggested that the clusters are stable from these studies.

For the doped solid hydrogen to be useful as HEDM, the impurity atoms must remain metastably trapped for a substantial lifetime. In addition, the concentration of the metastable impurity should be as high as possible. However, each system will have some maximal possible impurity concentration. This concentration, in principle, can be determined through a series of experiments, but uncontrollable experimental factors make it very difficult to correlate microscopic details of a system with its metastability in a quantitative and systematic way, so complementary simulation studies are useful.

A complete simulation study of the metastability of a quantum many-body system is a daunting problem. One must identify quantum metastable states in multidimensional space and adapt a suitable quantum dynamical simulation method or quantum rate theory. Only one model system is not enough to study as the information for various concentrations of the dopant are required.

The purpose of the present work is as follows: First, a qualitative global stability analysis of Li doped p-H_2 and B doped p-H_2 is carried out and an identification of metastable states with converging thermodynamic quantities will be made. For large scale model systems with varying concentration of the dopants, path integral molecular dynamics (PIMD)[11] simulations, an equilibrium finite temperature quantum simulation technique, are performed. The stability of the system is monitored along with the convergence of the thermodynamic quantities. Since PIMD is a fictitious time molecular dynamics simulation method, the lifetime determined by this method does not have a genuine physical meaning in real time. However, it can give an upper bound for the maximum metastable concentration and the qualitative estimation of the relevant thermodynamic quantities. This information is useful for the guidance of future experimental efforts to prepare samples and for more quantitative simulation studies.

Second, the pairwise reactivity of boron impurities in a solid

10.1021/jp992098d CCC: $18.00
Published on Web 10/30/1999

p-H_2 matrix will be studied. An earlier study on the recombination of Li impurities was carried out by two of us, and it was found that the Li atom shows significant quantum tunneling behavior and that the recombination reaction is estimated to be diffusion limited.[8] The boron counterpart of this study is performed here by constructing a quantum centroid potential of mean force (CPMF) at a globally stable impurity concentration.

Finally, the structural and dynamical effects of the pairwise boron impurity recombination on the rest of the system are studied. The pairwise reaction of two impurities may induce a structural change in the lattice and can release significant amounts of energy into the surrounding environment, both of which could in turn induce other impurity recombination reactions. Since the energy release process is a quantum dynamical process rather than an equilibrium process, the centroid molecular dynamics (CMD) method[12−15] will be used for this purpose. There have been previous CMD studies on pure solid p-hydrogen in our group[16] which showed that the calculated phonon spectrum is in good agreement with the experimentally observed spectrum, while the classical calculation resulted in very different results. Also, the self-diffusion constant of liquid p-hydrogen was calculated using CMD,[17] showing good agreement with experimental data. Recently, Kinugawa reported a CMD study on the dynamic structure factor of liquid p-hydrogen.[18]

The present paper is organized as follows: In section II a brief description is given of PIMD and CMD. The potential energies and calculation methods used in this study will also be presented in this section. Section III contains the simulation results and discussion, while concluding remarks are presented in section IV.

II. Methods

A. Path Integral Molecular Dynamics. The quantum canonical partition function Z has the following form

$$Z = \mathrm{Tr}[\mathrm{e}^{-\beta H}] \tag{1}$$

$$= \int \mathrm{d}\mathbf{q}\langle\mathbf{q}|\mathrm{e}^{-\beta H}|\mathbf{q}\rangle \tag{2}$$

where $\beta = 1/k_B T$ and H is the system Hamiltonian. Using indexed complete sets of coordinate and $\mathrm{e}^{-\beta H} = (\mathrm{e}^{-\epsilon H})^P$ with $\epsilon = \beta/P$, the partition function can be reexpressed as

$$Z = \prod_{i=1}^{P} \int \mathrm{d}\mathbf{q}_i \langle\mathbf{q}_i|\mathrm{e}^{-\epsilon H}|\mathbf{q}_{i+1}\rangle \tag{3}$$

Feynman showed that for a large enough number of discretizations P, this partition function can be described analytically in terms of quantum paths, i.e.

$$Z = (m/2\pi\hbar^2\epsilon)^{P/2} \prod_{i=1}^{P} \int \mathrm{d}\mathbf{q}_i \exp[-\beta V_{\mathrm{eff}}(q_i)] \tag{4}$$

where the effective potential $V_{\mathrm{eff}}(\mathbf{q})$ is given by

$$V_{\mathrm{eff}}(q_i) = \sum_{i=1}^{P}\left[\frac{mP}{2\hbar^2\beta^2}(q_i - q_{i+1})^2 + \frac{1}{P}V(q_i)\right] \tag{5}$$

In the limit $P \to \infty$, one obtains

$$Z = \int\cdots\int D\mathbf{q}(\tau) \exp\{-\mathbf{S}[\mathbf{q}(\tau)]/\hbar\} \tag{6}$$

with

$$\mathbf{S}[\mathbf{q}(\tau)] = \int_0^{\beta\hbar} \mathrm{d}\tau\left\{\frac{m}{2}\dot{\mathbf{q}}(\tau)^2 + V[\mathbf{q}(\tau)]\right\} \tag{7}$$

One can use PIMD generated by the effective potential in eq 5 to calculate the quantum equilibrium ensemble-averaged properties of the system.[11]

B. Centroid Molecular Dynamics. In CMD,[12−15] dynamical properties are calculated by classical-like equations of motion for the system path centroids, i.e.

$$m\frac{\mathrm{d}^2\mathbf{q}_c}{\mathrm{d}t^2} = -\nabla\vec{V}_c[\mathbf{q}_c(t)] \tag{8}$$

where $\mathbf{q}_c(t)$ is centroid coordinate of the system. The effective centroid potential $V_c(\mathbf{q}_c)$ is given by

$$V_c(\mathbf{q}_c) = -(1/\beta)\ln\left[\frac{\rho_c(\mathbf{q}_c)}{\rho_c^0(\mathbf{q}_c)}\right] \tag{9}$$

where $\rho_c^0(\mathbf{q}_c)$ is free particle centroid density, and $\rho_c(\mathbf{q}_c)$ is the centroid density for a given potential. The centroid density $\rho_c(\mathbf{q}_c)$ is given by

$$\rho_c(\mathbf{q}_c) = \int\cdots\int D\mathbf{q}(\tau)\delta(\mathbf{q}_c - \mathbf{q}_0)\exp\{-S[\mathbf{q}_i(\tau)]/\hbar\} \tag{10}$$

where $\mathbf{q}_0$ is particle centroid variable, defined as

$$\mathbf{q}_0 = \frac{1}{\hbar\beta}\int_0^{\hbar\beta} \mathrm{d}\tau\ \mathbf{q}(\tau) \tag{11}$$

Since the harmonic spring term of eq 5 gives poor sampling efficiency (especially if the number of discretization P is large), one can use the normal-mode transformation to diagonalize this term.[15,19] This can be done by Fourier expansion of the path, which is given by

$$\mathbf{q}_j = \sum_{n=1}^{P} \alpha_n \exp[2\pi i(j-1)(n-1)/P] \tag{12}$$

with normal mode α_n.[19] The normal modes α_n are complex with the following properties

$$\alpha_1 = R(\alpha_1) \tag{13}$$

$$\alpha_{P/2+1} = R(\alpha_{P/2+1}) \tag{14}$$

$$\alpha_n = \alpha_{P+2-n}^* \qquad (n = 2, ..., P/2) \tag{15}$$

where R here stands for the "real part of" and I stands for the "imaginary part of" below. Redefining the normal-mode coordinates as (with P even)

$$\mathbf{a}_1 = \alpha_1 \tag{16}$$

$$\mathbf{a}_P = \alpha_{P/2+1} \tag{17}$$

$$\mathbf{a}_{2n-2} = \sqrt{2}R[\alpha_n] \qquad (n = 2, ..., P/2) \tag{18}$$

$$\mathbf{a}_{2n-1} = \sqrt{2}I[\alpha_n] \qquad (n = 2, ..., P/2) \tag{19}$$

The final expression for the harmonic spring potential in terms of the normal-mode coordinate α_j is given by

$$\sum_{i=1}^{P}\frac{mP}{2\hbar\beta}(\mathbf{q}_{i+1}-\mathbf{q}_i)^2=\frac{mP}{2\hbar\beta}\sum_{n=1}^{P}\lambda_n\mathbf{a}_j^2 \qquad (20)$$

where $\lambda_1 = 0$, $\lambda_P = 4P$ and

$$\lambda_{2n-1}=\lambda_{2n-2}=2P[1-\cos(2\pi[n-1]/P)] \qquad (21)$$

It should also be noted that once the effective centroid potential in eq 9 is associated with a reaction coordinate and all other centroids of the system are integrated over, the reaction rate can be estimated by path integral quantum transition state theory (PI-QTST)[20−24] which is based on the centroid potential of mean force (CPMF) for the reaction coordinate. The calculation of the CPMF as a function of the reaction coordinate involves the direct calculation of its derivative and then the integration of this quantity over the reaction coordinate values of interest. Such a procedure for lithium impurity recombination is described in a previous paper,[8] and the same procedure is used here for boron impurities.

C. Potential Energy Functions. The Silvera−Goldman potential[25] was used for the H_2-H_2 interaction as in previous studies.[4−7] For the p-H_2/Li studies, the H_2−Li and Li−Li interactions were represented by Cheng and Whaley's[6] and Jang and Voth's[8] potentials, respectively. For the p-H_2/B studies, Alexander and Wang[26] calculated the H_2−B potential energies and generated an analytical expression by averaging over three different orientations of the 2p orbitals of the boron atom with respect to the p-H_2 molecule. The resulting potential has the fitted form

$$v(r)=c_1\exp(-\lambda_1 r)+(c_2+c_3 r)\exp(-\lambda_2 r)-\frac{c_4}{2r^6}[\tanh\{1.2(r-\lambda_3)\}+1] \qquad (22)$$

where $c_1 = -7.7200 \times 10^3$ cm^{-1}, $c_2 = -5.0553 \times 10^6$ cm^{-1}, $c_3 = 2.4887 \times 10^6$ cm^{-1}/Å^{-1}, $c_4 = -5.5570 \times 10^5$ cm^{-1}/Å^{-6}, and $\lambda_1 = 6.7219 \times 10^{-1}$ Å^{-1}, $\lambda_2 = 1.7967$ Å^{-1}, $\lambda_3 = 7.3479$ Å. The interactions of the boron impurities with the hydrogen lattice were approximated by pairwise summation over these isotropic model potentials.

There have been several studies on the B−B potential energy surfaces by both experiment and theory.[27−30] The ground state electronic potential is $X^3\Sigma_g^-$ and the next high-lying electronic state is $I^5\Sigma_u^-$.[29] The potential energy difference between these two states is several orders of k_BT at the potential minimum (1.590 16 Å) and the difference increases dramatically as the dimer distance is increased. There is curve crossing around 1.46 Å, but once the boron pair undergoes recombination reactions, the sampling of the potential energy contribution from the boron−boron distances less than equilibrium dimer distance should be ignorable. Recently, there has been new ground state ab initio calculations by Peterson et al.[31] at the val-CAS-ICMRCI (complete active space−internally contracted multi-reference configuration interaction)/cc-pCV5Z all-electron correlated level, which are the most recent and accurate results. The data is available only near the potential minimum. Their results were used to construct an analytical boron−boron potential using a Morse-like potential form, the Varshni function. The fitted potential is given by

$$v(r)=D_0[1-(r_0/r)\exp\{-\alpha(r^2-r_0^2)\}]^2-D_0 \qquad (23)$$

where $D_0 = 23\,475.49$ cm^{-1}, $r_0 = 1.590\,16$ Å, and $\alpha = 3.304 \times 10^{-2}$ Å^{-2}. Another ab initio calculation by Dupuis and Liu[27] shows almost the same behavior as our fitted potential. Figure 1 shows the fitted analytical potential for the boron−boron interaction against the ab initio data of both Peterson et al. and Dupuis and Liu. The Li−Li and H_2−B interaction potentials are also shown for comparison.

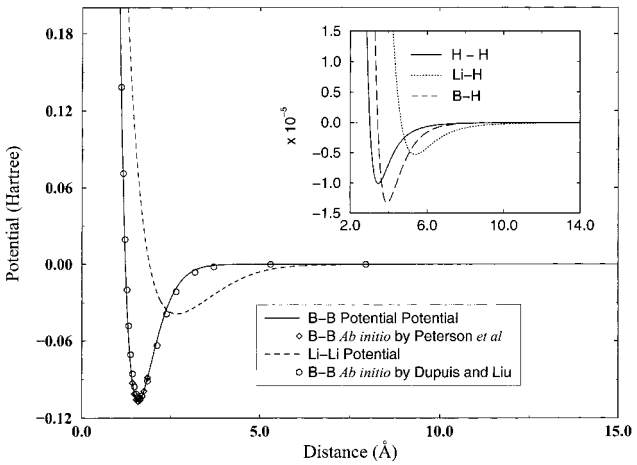

Figure 1. Various potential energy functions. The analytical boron−boron interaction potential is compared with ab initio data.

D. Simulation Details. The velocity Verlet (VV-I)[32] algorithm was used as an integrator of the thermostated dynamical equations of motion. The number of quantum discretizations P ("pseudo particles") was set at 48.[4−8] Nosé−Hoover chain dynamics[19,33−35] were used to keep the system at a constant temperature. Nosé−Hoover chains of length 4 were attached to each normal mode in each Cartesian direction of the pseudoparticles.[32,36−38] The simulation temperature was 4 K throughout the simulation.

This study required simulations of systems of large size with numerous initial trials under varying conditions, which proved to be computationally demanding. Especially the calculation of the CPMF and the CMD simulations required large amounts of averaging. To help overcome these difficulties, extensive parallel computations were used in all the calculations.

1. Global Stability Simulations for Lithium and Boron Impurities in Solid Hydrogen. To perform a stability analysis and to obtain an estimate of the maximum impurity doping densities for lithium and boron in solid hydrogen, it was necessary that the system be large enough to contain a reasonable number of impurities in the solid parahydrogen matrix. Large PIMD simulations with 1440 total particles were therefore used for this purpose.

Since solid parahydrogen has a large compressibility, there will be some global volume change after the dopants are trapped. Conventional constant pressure MD[39,40] was employed to treat this situation properly. Nosé−Hoover chains were implemented with a constant pressure simulation box wall. Pure solid parahydrogen has a hexagonal cubic packing structure (hcp). Independent scaling of the three orthogonal directions was allowed to accommodate the anisotropic nature of this lattice structure. The external pressure was then set to zero. The simulation parameters were adjusted to maximize the speed of convergence. If they are within reasonable range, the simulation parameters do not affect the simulation results. Table 1 lists the simulation parameters used.

The initial equilibrium configuration of the pure parahydrogen was generated starting from the hcp lattice structure with simulation box lengths of 38.20, 39.70, and 37.43 Å in the three orthogonal directions, respectively. This corresponds to the experimental density of pure solid parahydrogen of 23.1 cm^3/

TABLE 1: Simulation Parameters

system	time step (t_s)[a]	Nosé−Hoover mass[b]	wall mass[b]	Nosé−Hoover mass of wall[b]
H_2/Li	0.02	5.0	50.0	50.0
H_2/B	0.007	20.0	200.0	200.0

[a] The time step is given by $t_s = \hbar\beta/(4P)^{1/2}$, where P is number of PIMD pseudoparticles. [b] Masses are in units of $t_s^2/(2\pi^2\beta)$ (see Appendix).

mol. It took about 4.0 ps of PIMD time, which is about 5000 iterations, to reach equilibrium. The average box size of pure solid parahydrogen after it has reached equilibrium was 37.94, 39.45, and 37.19 Å. The configuration of the impurity-doped parahydrogen was then generated by replacing selected hydrogen molecules in the equilibrated pure solid hydrogen with the same number of impurities. Starting from this configuration, parahydrogen with impurities then evolved under further isothermal and isobaric PIMD simulation for a long enough time to reach "equilibrium", even though this metastable state could be valid only within the simulation time. A series of different impurity concentrations was then studied by changing the amount of trapped impurities systematically.

2. Intrinsic Recombination Rate Calculations for Boron Impurities in Solid Hydrogen. It is possible that recombination reactions might occur in the p-H_2/B system on a time scale much longer than that of the global stability simulations, and that such recombinations could trigger global instabilities in the lattice. Therefore, two B impurities were forced to recombine in a 6.25 mol % p-H_2/B system to study this possibility. PI-QTST simulations were[20−24] used for this purpose.

The reaction coordinate for the recombination of boron impurities in solid p-hydrogen matrix was defined as the boron−boron separation, and the CPMF was calculated as a function of this distance. The same method was followed as in previous work[8] on lithium impurity recombination except that the normal-mode transformation[15] was used to speed up the convergence of the path integral simulations.

In these simulations, the system consisted of 1152 particles in total. Starting from a perfect hcp lattice structure, the PIMD simulations were first performed under constant temperature and pressure as described above. The equilibrium structure of the pure solid p-H_2 was generated after 10 000 PIMD iterations (about 9.7 ps of PIMD time).

Instead of placing just two reacting impurities in the hydrogen simulation cell as in ref 8, in these simulations 72 hydrogen molecules were replaced with the same number of boron impurity atoms. The concentration of this system was 6.25 mol % boron, which is a stable concentration according to a large scale PIMD stability study similar to those described in the previous section. The box length after reaching equilibrium with 5000 PIMD iteration was 58.75, 75.40, and 71.21 Å. A pair of boron atoms in the direction of the longest box length was then chosen for the PMF calculation at this equilibrium configuration. Constant temperature and constant volume normal mode PIMD (NMPIMD)[11,32,39,40] was used for the calculations.

The equilibrium configurations of the system at different recombining boron pair distances (reaction coordinate) were quasistatically generated by increasing/decreasing the pair distance followed by 2500 NMPIMD iterations. The distance change was 0.0529 Å and the NMPIMD iterations were performed with a centroid distance constraint between the selected boron atoms during this procedure. All other boron atoms were free to move during the simulations. The mean force was calculated with a separation interval of 0.397 Å or less if necessary. A total of 25 000 normal-mode PIMD samplings were performed at each reaction coordinate for the PMF calculation. The number of sampling steps was increased to up to 75 000, depending on the reaction coordinate value, to ensure good convergence of the calculated PMF.

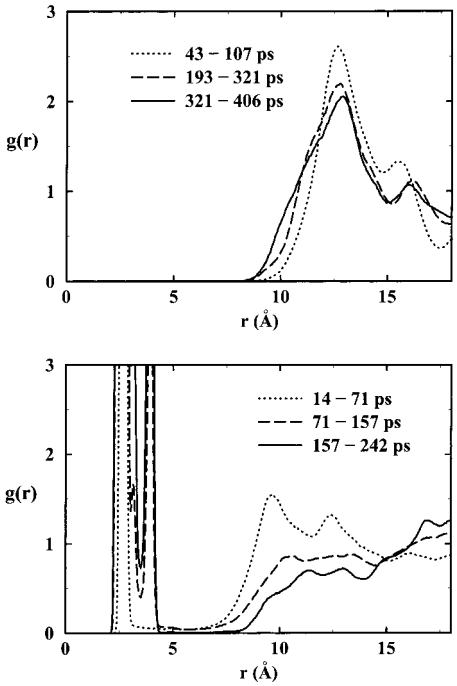

Figure 2. Time-dependent Li−Li pair distribution functions for 2.5 mol % (upper panel) and 3.3 mol % (lower panel) impurity concentrations.

3. Energy Disposal Calculations for Boron Impurities in Solid Hydrogen. The energy disposal dynamics during boron recombination was studied using CMD at 6.25 mol %, i.e., the same concentration as in the PI-QTST intrinsic recombination rate calculations. Due to the computational cost, the system was reduced to 432 particles in total of which 27 were boron impurities. The equilibrium configuration was generated by the same method as described in the previous section except for a different system size. The simulation box size after equilibration was 22.92, 19.85, and 37.43 Å.

The initial CMD configuration was prepared by quasistatically reducing the distance of a selected boron pair until it reached 5.39 Å, which is the barrier top for the recombination reaction as determined from the PI-QTST study. Then, CMD simulations were performed by starting the boron pair slightly to the product side from the top of the CPMF barrier. The boron pair distance was reduced by 0.01 Å from the barrier top to accomplish this.

The PIMD time step for solid hydrogen with boron impurities is about 0.25 fs. The CMD time step was correspondingly 0.0125 fs and the number of centroid force samplings was 10 at every CMD time step. A single CMD trajectory was calculated and the energies and structure of the system were monitored as a function of the CMD simulation time.

III. Results and Discussion

A. Global Stability Calculations for Lithium and Boron Impurities in Solid Hydrogen. In the simulations of the p-H_2/Li system, it was found that 36 Li atoms (2.5 mol %) with 1404 hydrogen molecules remain stable on the time scale of the simulation. The upper panel of Figure 2 shows the Li−Li pair distribution function sampled at different PIMD time intervals. The minimum distance that has a nonzero value in the pair

TABLE 2: Thermodynamic Quantities of the 2.5 mol % p-H_2/Li System[a]

simulation time (ps)	T_h/N_h	T_l/N_l	V_{hh}/N_h	V_{hl}/N_l	V_{ll}/N_l	E_l/N_l	vol/vol$_0$
43−107	53	31	−124	−413	−12	−394	1.21
107−192	54	31	−125	−428	−12	−410	1.21
107−320	54	31	−125	−436	−13	−419	1.21

[a] Energies are in K. T_h is the average kinetic energy of H_2; T_l is average kinetic energy of Li; V_{hh}, V_{hl}, and V_{ll} are the average interaction energies of H_2-H_2, H_2-Li, and Li−Li, respectively; N_h and N_l are number of H_2 and Li, respectively; E_l/N_l gives the total released energy per Li atom; vol/vol$_0$ is the ratio of the final system volume to the pure hydrogen volume.

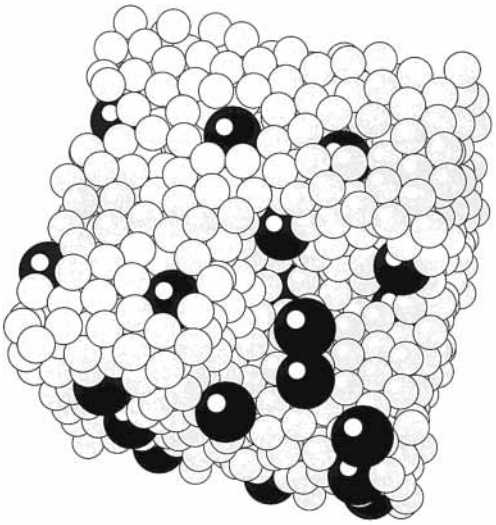

Figure 3. Snapshot of 34 Li atoms (2.5 mol %) in 1406 hydrogen molecules after 406 ps PIMD simulation time.

TABLE 3: Thermodynamic Quantities for the 3.3 mol % p-H_2/Li System[a]

simulation time (ps)	T_h/N_h	T_l/N_l	V_{hh}/N_h	V_{hl}/N_l	V_{ll}/N_l	E_l/N_l	vol/vol$_0$
0−14	49	30	−116	−342	−35	−347	1.28
14−71	53	39	−120	−374	−3249	−3584	1.25

[a] Definitions are the same as in Table 2.

distribution function is 7.8 Å. Table 2 lists various thermodynamic quantities calculated at this concentration. Both the upper panel of Figure 2 and Table 2 indicate that there is no Li−Li recombination reaction and it has reached equilibrium; i.e., the trapped Li atoms remain in a metastable state during the tested interval of time. Figure 3 shows a configuration of the 2.5 mol % system from near the end of the simulation.

The same calculation with 48 Li atoms (3.3 mol %) showed that the system is not stable and Li−Li recombination reactions begin to occur on a short time scale. The lower panel of Figure 2 is the Li−Li pair distribution function at different times of PIMD simulation. As the recombination reaction progresses, energy begins to be released mainly due to the strong Li−Li interaction potential. The amount of energy released during the two time intervals is listed in Table 3 along with other thermodynamic quantities. The large peaks in the pair distribution function at distances less than 8.0 Å in the lower panel of Figure 2 clearly show the degree of recombination reactions at this concentration, which begins a cascade process. The potential of mean force calculation by Jang and Voth[8] shows that the Li−Li recombination barrier top is at impurity distances of about 8.28 Å. Even though their calculation was performed at a much lower concentration, the present study is in qualitative agreement

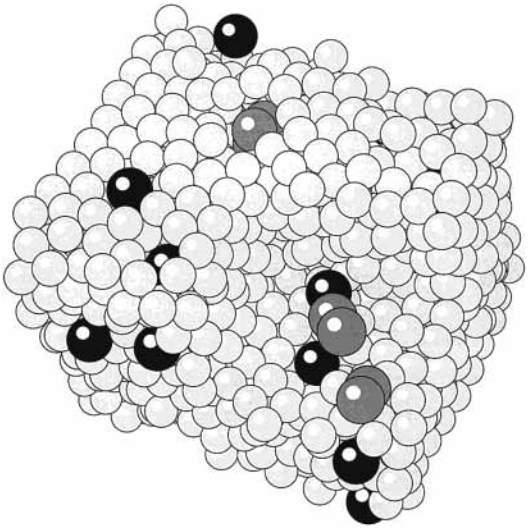

Figure 4. Snapshot of 48 Li atoms (3.3 mol %) in 1392 hydrogen molecules after 242 ps PIMD simulation time. The recombined lithium atoms are shaded in gray.

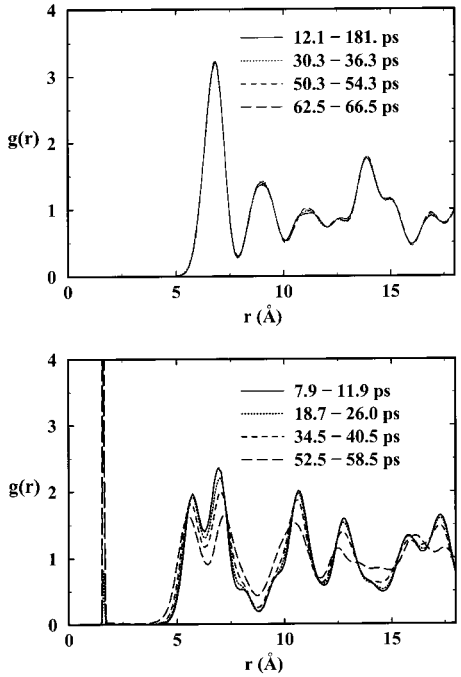

Figure 5. Time-dependent boron−boron pair distribution functions for 15.0 mol % (upper panel) and 25.0 mol % (lower panel) impurity concentrations.

with their results. Figure 4 shows a configuration of the 3.3 mol % system near the end of the simulation. Note the recombined lithium impurities.

The boron−boron pair potential is much shorter ranged and more attractive than the Li−Li interaction potential, while the H_2-B interaction is shorter ranged and deeper than that of H_2-Li (cf. Figure 1). As a result, more boron atoms are expected to be metastably trapped than Li atoms. The simulations indeed show that 216 boron atoms (15.0 mol %) in 1224 p-H_2 molecules remain stable on the time scale of the simulation, while 360 boron atoms (25.0 mol %) in 1080 p-H_2 molecules do not. The time-dependent boron−boron pair distribution functions at these concentrations are shown in Figure 5.

The long-range region of the model boron−boron potential might influence the results of the present calculations, but the boron−boron potential is a fairly short-ranged interaction, which

TABLE 4: Thermodynamic Quantities for the 15 mol % p-H_2/B System[a]

simulation time (ps)	T_h/N_h	T_b/N_b	V_{hh}/N_h	V_{hb}/N_b	V_{bb}/N_b	E_b/N_b	vol/vol$_0$
18.1−24.1	64	19	−116	−480	−0.12	−461	1.10
30.2−36.3	64	25	−116	−480	−0.16	−455	1.10
50.4−54.4	64	24	−116	−480	−0.16	−456	1.09
62.5−66.5	64	23	−112	−452	−0.20	−388	1.09

[a] Definitions are the same as in Table 2.

TABLE 5: Thermodynamic Quantities of the 25 mol % p-H_2/B System[a]

simulation time (ps)	T_h/N_h	T_b/N_b	V_{hh}/N_h	V_{hb}/N_b	V_{bb}/N_b	E_b/N_b	vol/vol$_0$
3.0−7.9	64	25	−92	−416	−0.60	−391	1.19
26.0−32.2	64	20	−92	−420	−544	−940	1.17
46.5−52.5	64	29	−92	−420	−2360	−2743	1.15

[a] Definitions are the same as in Table 2.

is well characterized by our fitted potential. It is therefore expected that there would be no qualitative change due to errors in the long-range tail. There might be another more serious error caused by using a model H_2-B potential which is isotropic and does not have the dependence on the orientation of the 2p boron orbitals. However, considering the condensed phase environment and dynamic fluctuations of the hydrogen matrix which average the interaction around each boron, the use of the isotropic potential may be justified.

It should also be pointed out that the present simulations do not consider vacancy sites which might play an additional role in the stability issue. The impurities are initially arranged such that they make a uniform distribution at a given concentration. During the actual experimental deposition of impurities, there might be an irregular distribution of impurities and some reacted species which may induce local or global reactions. It is important that the number of impurities in the present case be understood as an upper bound for the stability of the system. The 216 boron atoms (15.0 mol %) case is certainly only a threshold density. For more highly concentrated systems, the time-dependent pair distribution function shows boron pairs with less than 4.3 Å separation readily undergo recombination reactions. The minimum distance between boron impurities in the 15.0 mol % system is 4.59 Å. Considering the lattice constant of pure solid p-H_2 is about 3.5 Å, this is a rather short distance. The thermodynamic data for the two p-H_2/B calculations with 216 B atoms and 360 B atoms are listed in Tables 4 and 5, respectively. Also shown in Figures 6 and 7 are snapshots of the p-H_2/B simulations at the final states showing their stability and/or instability.

The p-H_2/B systems have a considerably higher impurity concentration than p-H_2/Li in its metastable state. It is therefore likely that B is potentially more useful than Li for creating high energy density matter. The small size of the B atom contributes to this extra stability, causing less distortion of the solid p-H_2 matrix than the Li atom. This can be seen from Tables 2 and 3. The total volume of the system changes slightly for the 15 mol % p-H_2/B system even though its impurity concentration was 6 times greater than that for the 2.6 mol % p-H_2/Li system. The $B-H_2$ interaction potential is also much more attractive than the $Li-H_2$ potential (cf. inset in Figure 1) and not much different than the H_2-H_2 potential. This suggests that B atoms may go into substitutional defects in the p-H_2 lattice readily.

In the present work, chemical reactions of the impurity atoms with the hydrogen molecules were not considered. Recent experimental results show that a boron atom can undergo an

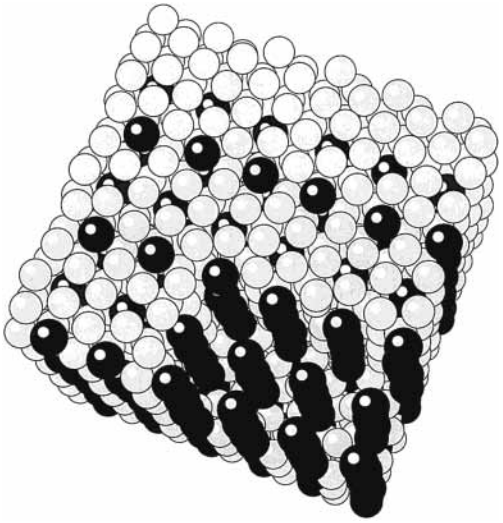

Figure 6. Snapshot of 216 B atoms (15 mol %) in 1224 hydrogen molecules after 78 ps PIMD simulation time.

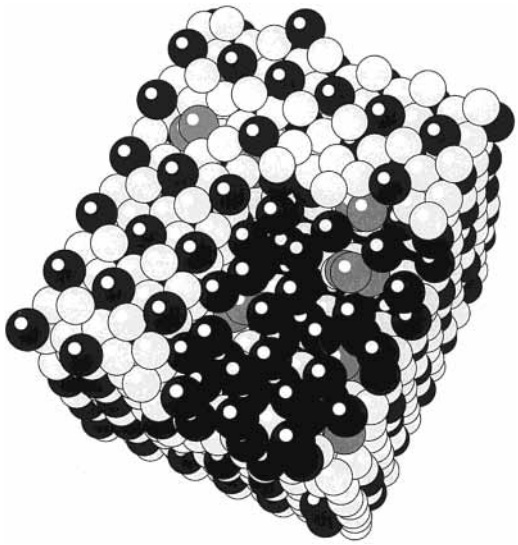

Figure 7. Snapshot of 360 B atoms (25 mol %) in 1080 hydrogen molecules after 59 ps PIMD simulation time. The recombined boron atoms are shaded in gray.

insertion reaction.[1−3] According to ab initio calculations for cluster systems,[41,42] the activation energy barrier for such a reaction is about 80 kJ/mol, which is much higher than the thermal energy at 4 K. It should also be noted that only single initial configurations of the impurity systems were studied due to the computationally demanding nature of the simulations. A more systematic study will be the subject of future research.

B. Intrinsic Recombination Rate Calculations for Boron Impurities in Solid Hydrogen. Figures 8 and 9 show the computed centroid mean force and centroid potential of mean force, respectively, for the recombination reaction of two boron impurities. The overall statistical error of the calculated potential of mean force is about 10%. The transition state is at 5.39 Å and there is an abrupt change of the centroid force (and thus the CPMF) toward the impurity recombination after the transition state. This is because there is a significant onset of quantum tunneling of the borons as pointed out in previous work on impurity recombination.[8] The calculated barrier height is 350 ± 35 K. As can be seen in Figure 1, the $B-H_2$ well depth is 3 times deeper than the $Li-H_2$ potential, and the latter has more repulsive energy within the H_2 lattice owing to its large size. Therefore, it may not be surprising that the barrier for intrinsic

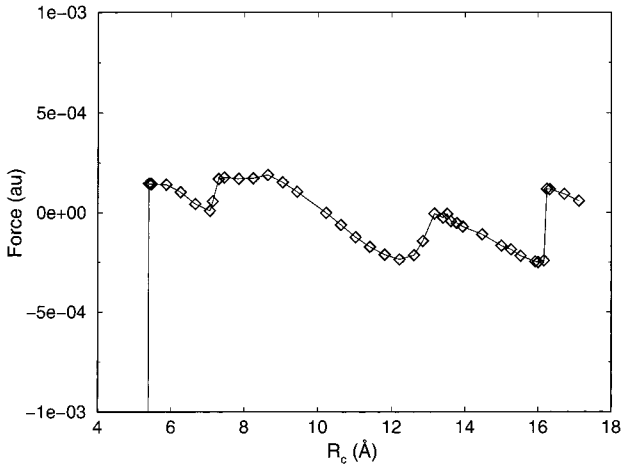

Figure 8. Centroid mean force as a function of centroid distance R_c between two boron impurities at 6.25 mol %. Note that force at 5.36 Å is not shown here which is -1.09×10^{-2}.

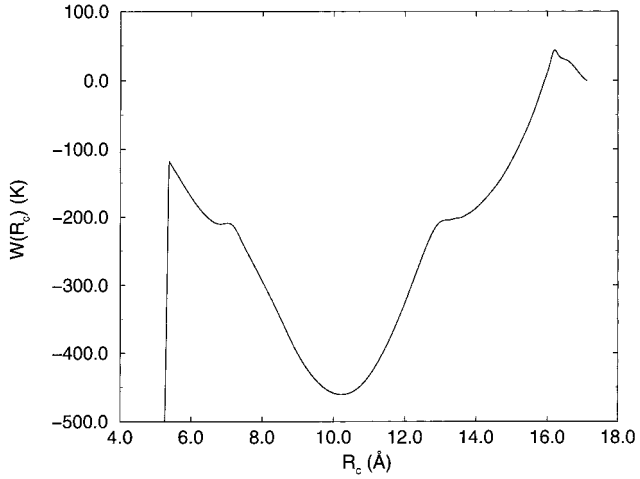

Figure 9. Centroid potential of mean force (CPMF) from integration of Figure 8.

recombination of Li in solid H_2 is 4 times less (80 K) than that for boron.[8] The other abrupt changes in the CPMF away from the barrier region are due to lattice rearrangements in the vicinity of the recombining impurities.

Using the same analysis as in a previous study,[8] the quantum intrinsic reaction rate is estimated to be 8×10^{-27} s^{-1}. Considering the error in the calculated CPMF, the intrinsic rate range is 1×10^{-30} to 7×10^{-24} s^{-1}. The rate of impurity recombination can then be described in terms of the intrinsic recombination rate and the diffusion rate.[43−45] Following the same analysis as for the Li reaction rate,[8] the intrinsic recombination rate is estimated from the intrinsic reaction rate to be 2×10^{-46} cm^3 s^{-1}. This extremely slow intrinsic reaction rate can be compared with the estimated self-diffusion rate which is 2×10^{-30} cm^3 s^{-1} if boron has the same self-diffusion rate as pure solid hydrogen. Based on the above qualitative arguments, it can be suggested that in a perfect solid the overall boron recombination reaction rate is limited by the intrinsic recombination step (unlike lithium which was estimated to be a diffusion-limited reaction[8]). The forced recombination of two boron impurities at the 6.25 mol % concentration results in only local recombination of three boron atoms, not global instability, as will be further discussed at the end of the next section.

Of course, in a real solid there will be defects, grain boundaries, etc., which may influence the intrinsic recombination rates. The effects of these will be the subject of future research.

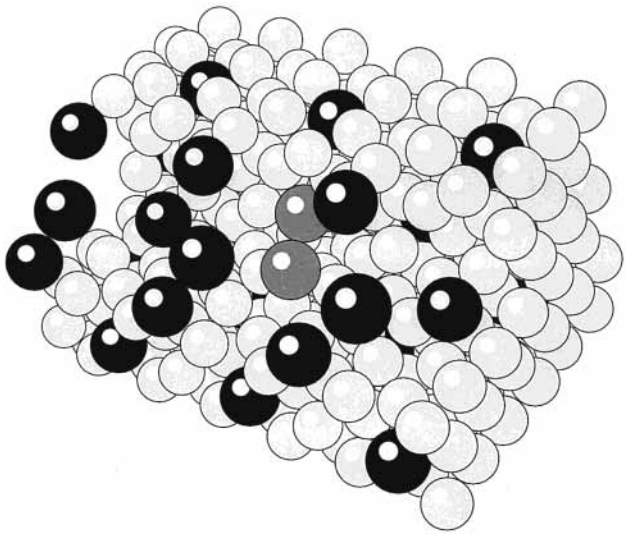

Figure 10. Snapshot of 405 hydrogen molecules and 27 boron atoms (6.25 mol %) before the CMD simulation.

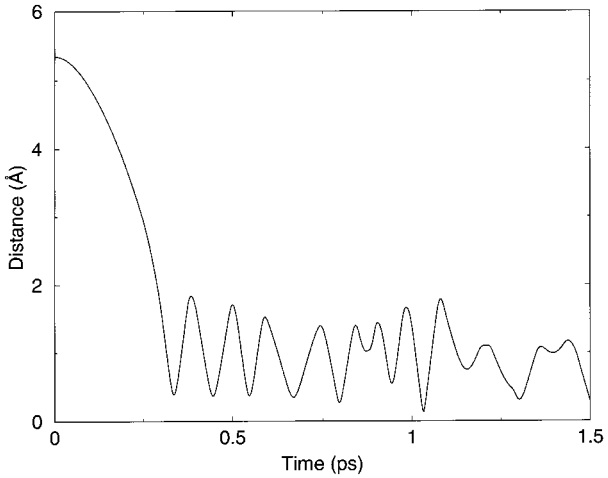

Figure 11. Centroid distance of the selected recombining boron pair as a function of time. Plotted is the distance as a function of the equilibrium B−B distance from Figure 1.

It should also be noted that the current calculation was at only one particular boron concentration. Furthermore, the selected boron pair represents only one possible reacting configuration in the ordered solid hydrogen matrix at the specified concentration.

C. Energy Disposal Calculations for Boron Impurities in Solid Hydrogen. As can be seen from the B−B potential energy function in Figure 1, a boron pair recombination will release a significant amount of energy during the recombination event. It was therefore important to study the dynamical effects of the boron recombination on the overall system stability using a CMD simulation. The released energy may trigger other nonequilibrium recombination reactions of adjacent boron atoms which could produce a cascade effect of recombination reactions. This is certainly true at higher impurity concentrations as seen from the global stability simulations at 25 mol %.

Figure 10 shows the system configuration before the CMD simulation was started. The change of centroid distance between the selected recombination pair of boron atoms (gray atoms in Figure 10) is shown in Figure 11 as a function of time. Plotted is the interpair B−B distance. The distance change is large at the early stage of the CMD simulation as the pair rapidly releases its energy to the environment (hydrogen and other

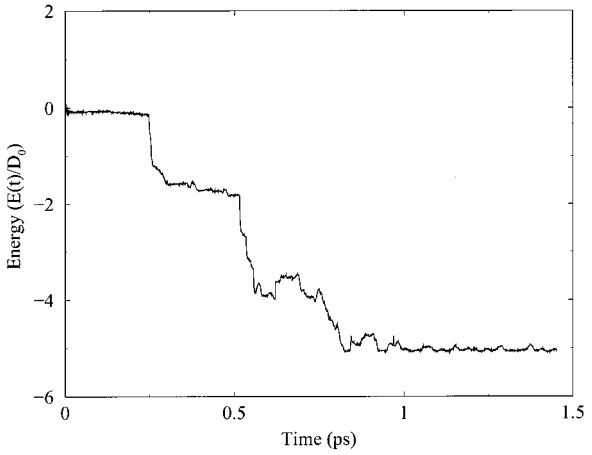

Figure 12. Released energy as a function of time for the recombining B−B pair. Plotted is the released energy as a function of the B−B well depth from Figure 1.

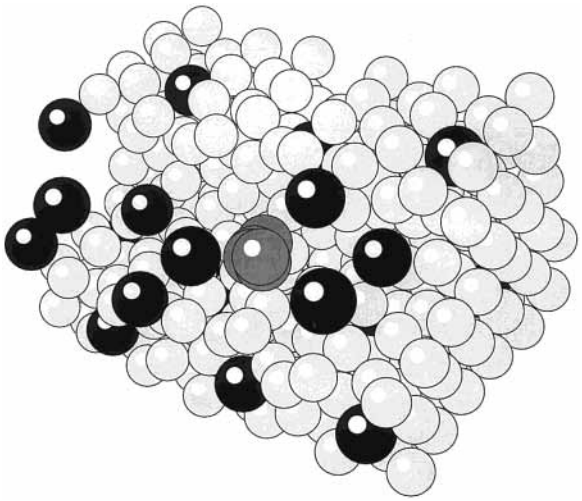

Figure 13. Snapshot of 405 hydrogen and 27 boron atoms (6.25 mol %) after 1.6 ps of CMD simulation. The locally recombined boron atoms are shown.

borons). Figure 12 shows the total energy of the boron impurities in the system as a function of time (as a fraction of a single B−B well depth). As one can see both from the boron pair distance change and from the energy release plots, the time scale by which the boron pair releases a significant amount of energy to the environment is around 0.25 ps at this impurity concentration. The released energy from the first recombination helps to trigger further local recombination reactions with other nearby boron impurities within the simulation time scale and thereby changes the local solid structure. The "stair step" nature of the boron impurity energy as a function of time in Figure 12 shows the recombination of other local impurities with the initially recombining pair to form a more stable cluster of five borons at larger time scales (greater than 1 ps). It is interesting to note the very short time scale of each additional recombination event in Figure 12. Figure 13 shows a snapshot of the system after 1.75 ps. The five boron impurities shaded in gray are seen to have undergone a local recombination process, but the global structure of the system is unchanged at this concentration. These results are consistent with those from the PI-QTST simulations described in the last section. The actual number of borons included in the local cluster may differ due to the approximate nature of the pair potential that we have used (i.e., we have ignored the many-body effects) but the qualitative picture should remain the same.

Finally, it should be mentioned that the forced recombination of a boron pair is a nonequilibrium process and that CMD is clearly approximate in this situation.

IV. Concluding Remarks

In this paper, solid parahydrogen systems doped with lithium and boron impurities have been studied. Both the global stability simulations and the computed thermodynamic properties show that boron is a more effective impurity than lithium in a solid hydrogen matrix for HEDM purposes since the concentration stability threshold for boron is estimated to be at least twice that of lithium. These results also suggest that a realistic concentration of boron impurities cannot likely exceed 10 mol %. It was found that the boron recombination reaction rate may be limited by the intrinsic recombination reaction rather than the impurity self-diffusion process. The dynamical CMD simulations and PI-QTST calculations at 6.25 mol % show that the reaction of a single boron pair induces only local boron recombinations and may not induce a global instability. The present results therefore support the concept that the p-H_2/B system may eventually represent a useful form of HEDM.

Acknowledgment. This research was supported by the Air Force Office of Scientific Research. We thank Kirk Peterson for providing his ab initio results, Youngshang Pak for helping in the construction of the potential energy surface, and Millard Alexander for providing the H_2−B interaction potential. The calculations were carried out through a DOD Challenge Grant at the Maui High Performance Computing Center on the IBM SP2, and on the SGI Origin 2000 at NCSA and IBM SP2 and Cray T3E at The San Diego Supercomputing Center through an NSF MetaCenter computing grant. Parts of the calculation were also performed on the IBM SP2 at the Center for High Performance Computing (CHPC) at the University of Utah. The SP2 was partially funded by an NSF grant CDA 9601580 and a Shared University Research (SUR) grant from IBM.

Appendix: Constant Pressure MD with a Nosé−Hoover Chain Thermostat

In Andersen's constant-pressure MD method, the volume of the simulation box is allowed to fluctuate by introducing an extended Lagrangian. In this view, the volume of the system is changed by a piston (wall) with a fictitious mass. The Nosé−Hoover chain is then attached both to the atomic particles and to the fictitious wall.[46]

After the atomic particle coordinate r_i is replaced with scaled coordinate $\rho_i = Q^{-1/3} r_i$, where Q is volume, the extended Lagrangian of the system is given by

$$L = \sum_{i=1}^{N} {}^1/_2 m_i Q^{2/3} \eta_{1(i)}{}^2 \dot{\rho}_i{}^2 - V(\rho_i Q^{1/3}, i = 1, ..., N) + {}^1/_2 M_Q \xi_1 \dot{Q}^2 - P_{\text{ext}} Q + \sum_{j=1}^{K} {}^1/_2 M_{\xi_j} \dot{\xi}_j{}^2 - g k_B T \zeta_1 - \sum_{j=2}^{K} k_B T \zeta_j + \sum_{i=1}^{N} \left(\sum_{j=1}^{K} {}^1/_2 M_{\eta_{j(i)}} \dot{\eta}_{j(i)}{}^2 - g k_B T \eta_{1(i)} - \sum_{j=2}^{K} k_B T \eta_{j(i)} \right) \quad \text{(A1)}$$

where m_i is the mass of the atomic particle, N is total number of particles, V is potential of the system, M_Q is mass of the fictitious wall, P_{ext} is the external pressure, ζ_j is the position of the jth Nosé−Hoover chain attached to wall, M_{ζ_j} is the mass of the jth Nosé−Hoover chain attached to wall, K is the number of Nosé−Hoover chains, g is the degree of freedom of the

Nosé−Hoover chain attached to a given object, $\eta_{j(i)}$ is the position of the *j*th Nosé−Hoover chain attached to the *i*th atomic particle, and $M_{\xi_{j(i)}}$ is the mass of the *j*th Nosé−Hoover chain attached to the *i*th atomic particle.

One can then derive the equations of motion of the system. In the resulting expression, the Nosé−Hoover chain attached to the atomic particles is different from the Nosé−Hoover chain attached to the fictitious wall, and each atomic particle has its own Nosé−Hoover chain.

References and Notes

(1) Fajardo, M. E.; Carrick, P. G.; Kenney III, J. W. *J. Chem. Phys.* **1991**, *5812*, 94.
(2) Fajardo, M. E. *J. Chem. Phys.* **1993**, *110*, 98.
(3) Fajardo, M. E.; Tam, S.; Thompson, T. L.; Cordonnier, M. E. *Chem. Phys.* **1994**, *351*, 189.
(4) Li, D.; Voth, G. A. *J. Chem. Phys.* **1992**, *5340*, 96.
(5) Li, D.; Voth, G. A. *J. Chem. Phys.* **1993**, *5734*, 98.
(6) Cheng, E.; Whaley, K. B. *J. Chem. Phys.* **1996**, *3155*, 104.
(7) Scharf, D.; Martyna, G. J.; Li, D.; Voth, G. A.; Klein, M. L. *J. Chem. Phys.* **1993**, *99*, 9013.
(8) Jang, S.; Voth, G. A. *J. Chem. Phys.* **1998**, *4098*, 108.
(9) Gerber, R. B.; Li, Z.; McCoy, A. B. In *Proceedings of the High Energy Density Matter (HEDM) Contractors' Meeting, 6−8 June 1993, Woods Hole, MA*; Thompson, T. L. Ed.; USAF Phillips Laboratory: Edwards AFB, CA, 1993; PL-TR-93-3041.
(10) Vegiri, A.; Alexander, M. H.; Gregurick, S.; McCoy, A. B.; Gerber, R. B. *J. Chem. Phys.* **1994**, *101*, 2577.
(11) For reviews, see: (a) Berne, B. J.; Thirumalai, D. *Annu. Rev. Phys. Chem.* **1986**, *37*, 401. (b) Freeman, D. L.; Doll, J. D. *Adv. Chem. Phys. B* **1988** *70*, 139. (c) Doll, J. D.; Freeman, D. L. *Adv. Chem. Phys. B* **1989** *73*, 289. (d) Doll, J. D., Gubernatis, J. E., Eds. *Quantum Simulation of Condensed Matter Phenomena*; World Scientific: Singapore, 1990. (e) Chandler, D. In *Liquides, Cristallisation et Transition Virtreuse, Les Houches, Session LI*; Levesque, D., Hansen, J. P., ZinnJustin, J., Eds.; Elsevier: New York, 1991.
(12) Cao, J.; Voth, G. A. *J. Chem. Phys.* **1993**, *10070*, 99.
(13) Cao, J.; Voth, G. A. *J. Chem. Phys.* **1994**, *5106*, 100.
(14) Cao, J.; Voth, G. A. *J. Chem. Phys.* **1994,** *6157*, 101.
(15) Cao, J.; Voth, G. A. *J. Chem. Phys.* **1994**, *6168*, 101.
(16) Calhoun, A.; Pavese, M.; Voth, G. A. Unpublished results.
(17) Calhoun, A.; Pavese, M.; Voth, G. A. *Chem. Phys. Lett.* **1996**, *415*, 262.
(18) Kinugawa, K. *Chem. Phys. Lett.* **1998**, *454*, 292.
(19) Martyna, G. J.; Klein, M. L.; Tuckerman, M. *J. Chem. Phys.* **1992**, *2635*, 97.
(20) Voth, G. A.; Chandler, D.; Miller, W. H. *J. Chem. Phys.* **1989**, *7749*, 91.
(21) Voth, G. A. *Chem. Phys. Lett.* **1990**, *289*, 270.
(22) Voth, G. A. *J. Phys. Chem.* **1993**, *8365*, 97.
(23) Gillan, M. J. *J. Phys. C* **1987**, *3621*, 20.
(24) Cao, J.; Voth, G. A. *J. Chem. Phys.* **1996**, *6856*, 105.
(25) Silvera, I. F.; Goldman, V. V. *J. Chem. Phys.* **1978**, *4209,* 69.
(26) Alexander, M. H.; Yang, M. *J. Chem. Phys.* **1995**, *9756*, 103.
(27) Dupuis, M.; Liu, B. *J. Chem. Phys.* **1978**, *2902*, 68.
(28) Deutsch, P. W.; Curtiss, L. A.; Pople, J. A. *Chem. Phys. Lett.* **1990**, *33*, 174.
(29) Hachey, M.; Karna, S. P.; Grein, F. *J. Phys. B: At. Mol. Opt. Phys.* **1992**, *1119*, 25.
(30) Martin, J. M. L.; Francois, J. P.; Gijbels, R. *Chem. Phys. Lett.* **1992**, *529*, 189.
(31) Peterson, K. A.; Wilson A. K.; Woon D. E.; Dunning, T. H., Jr. *Theor. Chem. Acc.* **1997**, *97*, 251.
(32) Jang, S.; Voth, G. A. *J. Chem. Phys.* **1997**, *9514*, 107.
(33) Nosé, S. *J. Chem. Phys.* **1984**, *511*, 81.
(34) Nosé, S. *Mol. Phys.* 1984, *255*, 52.
(35) Hoover, W. G. *Phys. Rev. A* **1985**, *1695*, 31.
(36) Tuckerman, M. E.; Berne, B. J.; Martyna, G. J.; Klein, M. L. *J. Chem. Phys.* **1993**, *2796*, 99.
(37) Tuckerman, M. E.; Parrinello, M. *J. Chem. Phys.* **1994**, *1302*, 101.
(38) Tuckerman, M. E.; Marx, D.; Klein, M. L.; Parrinello, M. *J. Chem. Phys.* **1996**, *5579*, 104.
(39) Andersen, H. C. *J. Chem. Phys.* **1980**, *2384*, 72.
(40) Parinello, M.; Rahman, A. *Phys. Rev. Lett.* **1980**, *1196*, 45.
(41) Alexander, M. H. *J. Chem. Phys.* **1993**, *6014*, 99.
(42) Alexander, M. H.; Vegiri, A. In *Proceedings of the High Energy Density Matter (HEDM) Contractors Conference, 6−8 June 1993, Woods Hole, MA*; Thompson, T. L., Ed.; USAF Phillips Laboratory: Edwards AFB, CA, 93524-5000, 1993; PL-TR-93-3041.
(43) Smoluchowski, M. *Z. Phys. Chem.* **1918**, *129*, 92.
(44) Collins, F. C.; Kimball, G. E. *Science* **1949**, *425*, 4.
(45) Noyes, R. M. *Prog. React. Kinet.* **1961**, *129*, 1.
(46) Ferrario, M. In *Computer Simulation in Chemical Physics*; Allen, M. P., Tildesley, D. J., Eds.; NATO ASI Series C.; Kluwer Academic Publishers: New York, 1993; Vol. 397.